Semi-empirical molecular orbital studies of porphine and phthalocyanine derivatives, to simulate their intermolecular interactions

ARTICLE *in* INTERNATIONAL JOURNAL OF QUANTUM CHEMISTRY · DECEMBER 1992

Impact Factor: 1.43 · DOI: 10.1002/qua.560460119

INTERNATIONAL JOURNAL OF QUANTUM CHEMISTRY, VOL. 46, 191–210 (1993)

Semi-empirical Molecular Orbital Studies of Porphine and Phthalocyanine Derivatives, to Simulate Their Intermolecular Interactions

TSVETAN G. GANTCHEV*
MRC Group in the Radiation Sciences, Faculty of Medicine, Université de Sherbrooke, Sherbrooke, Québec, Canada J1H 5N4

FRANCIS BEAUDRY
Structural Chemistry Laboratory, Faculty of Science, Université de Sherbrooke, Sherbrooke, Québec, Canada J1K 2R1

JOHAN E. VAN LIER
MRC Group in the Radiation Sciences, Faculty of Medicine, Université de Sherbrooke, Sherbrooke, Québec, Canada J1H 5N4

ANDRÉ G. MICHEL
Structural Chemical Laboratory, Faculty of Science, Université de Sherbrooke, Sherbrooke, Québec, Canada J1K 2R1

Abstract

Ground-state electronic properties of porphine, phthalocyanine, and their derivatives, photosensitizers with potential use in the photodynamic therapy of tumors, were studied by semiempirical (MNDO) molecular orbital calculations. Geometry, bond orders, electron populations, and net atomic charges were analyzed. The obtained models were applied to study the intermolecular interactions of these molecules utilizing a classical mechanics approach. The dimerization characteristics of different derivatives were obtained by a separate evaluation of the contribution of electrostatic and steric factors. © 1993 John Wiley & Sons, Inc.

Introduction

Because of their biological significance and specific catalytic properties, the electronic structure of porphyrins and phthalocyanines has been extensively studied (reviewed in [1]). Numerous theoretical approaches have been utilized to explain

*On leave from Department for Cell and Molecular Biology of Cancer, National Centre of Oncology, Sofia, Bulgaria.

CCC 0020-7608/93/010191-20

the general features of porphyrin and phthalocyanine molecular organization: self-consistent field (SCF) calculations based on the Pariser–Parr–Pople π-electron method [2–4]; the iterative extended Hückel all-valence electron technique [5]; the semiempirical CNDO/2–SCF [6]; ab initio SCF calculations [7, 8]; and more recently, the valence effective Hamiltonian (VEH) method [9, 10].

The newly expanded interest in the photophysics and photochemistry of porphyrins and phthalocyanines is related to the capability of some derivatives to act as tumor-localizing photosensitizers for potential use in the photodynamic therapy of cancer [11]. In parallel with the triplet excited state-mediated efficiency of energy and/or electron transfer reactions, the biological activity of these molecules strongly depends on environmental factors, favorable (or not) for dye–dye ground-state dimerization (aggregation) and substrate complexation [12, 13]. In unsubstituted neutral porphyrin and phthalocyanine molecules, the ground-state complexation (aggregation) is determined by $\pi-\pi$ interactions. Substitution of the macrocycles with various polar side chains exerts additional electrostatic effects. Different models have been proposed to account for experimental observations of porphyrin and metalloporphyrin aggregation on the basis of $\pi-\pi$ attraction. Most of the early concepts consider donor–acceptor, atomic-charge, and/or solvophobic interactions [14–17]. Recently, a model based on compensatory contributions of $\pi-\pi$ and $\pi-\sigma$ repulsion/attraction also has been discussed [18].

In the present study, we investigated porphine–porphine and phthalocyanine–phthalocyanine interactions using computer modeling. As the first step, we performed quantum mechanical calculations to characterize the electronic properties of the molecules of interest. For large molecules such as porphyrins and phthalocyanines, a successful computation of their electronic structure is not a trivial problem. We used a semiempirical molecular orbital (MNDO, modified neglect of diatomic overlap [19, 20]) approach, imposing certain symmetry relations on appropriate atomic constrains. Ground-state properties were examined, and particular emphasis was placed on the geometry optimization and characterization of the bond orders, electron population, and net atomic charges. Comparison with literature experimental and theoretical data was made, as feasible. To provide further insight into the mechanism of intermolecular attraction and to keep the models as close as possible to biologically relevant systems, molecular structures differing by their net charge, protonation state, or metalation were implicated in the calculations. Several more complicated side-chain and heterocyclic-ring-substituted phthalocyanine models, including metallophthalocyanines with additional axial ligands, were also introduced.

The intermolecular interactions (formation of dimers) were evaluated by computing the minimum of the intermolecular energy in respect to the relative molecular orientation in space. The approach applied involved separate calculation of steric and electrostatic contributions in the energy of one of the partner molecules when introduced in the field of the other.

Molecules

The basic molecules in our model studies were unsubstituted porphine and phthalocyanine (porphyrazine). The input atomic coordinates for the first set of MNDO

calculations of the parent porphine and phthalocyanine skeletons were taken from relevant crystallographic data [21, 22], and the obtained coordinates were reintroduced for further geometry optimization. The following porphine molecules were computed: nonprotonated neutral porphine, P; dianion P^{2-}; dication (free acid) porphine, P^{2+}; neutral (free base) H_2–porphine, H_2P; Zn–porphine, ZnP; axially coordinated mono- and diaquo-Zn($2H_2O$)–porphine; and $GeCl_2$ or $Ge(OH)_2$–porphine. To evaluate the perturbations caused by electron-withdrawing atoms and/or their steric repulsion/attraction effects involved in intermolecular interactions, several *meso*-halogenated derivatives [$H_2P(4F)$; $H_2P(4Cl)$; $H_2P(4Br)$; and $H_2P(4I)$] were also calculated [23, 24]. The following computer models of phthalocyanine derivatives were studied: H_2–phthalocyanine, H_2Pc; Al–phthalocyanine, $AlPc^{1+}$, chloroaluminum–phthalocyanine, AlClPc; H_2–tetrasulfophthalocyanine, $H_2Pc(SO_3H)_4$; H_2-tetrasulfophthalocyanine tetraanion, $H_2Pc(SO_3)_4^{4-}$; and H_2–tetrapyridino–porphyazine, $H_2Pc(4N)$. The molecules were calculated introducing two- and/or four-fold (C_{2h}, D_{2h}, and D_{4h}) axes of symmetry. The minimized structures were practically planar with the exception of the $H_2P(4F)$, which showed a more pronounced tendency of out–off-plane bending. Out–off-plane coordinates of side-chain groups, metal ions, and axial ligands were used in input files.

Computational Details

Molecular orbital calculations were performed with the MOPAC software (versions from 5.1 to 6.0, [25]), on RISC 6000 workstations of the Laboratoire de Chimie Structurale & Modélisation Moléculaire of the University of Sherbrooke. The semiempirical molecular orbital calculation technique utilized was MNDO (modified neglect of diatomic overlap) with H, C, and N atom parametrization as described by Dewar and Thiel [19, 20]. The MNDO versions used also included parametrizations of other atoms of interest: Al [26], Cl [27], and Zn and Ge [28]. Atomic charges and bond orders were derived from Mulliken population analysis in terms of a separate evaluation of partial and total "net atomic populations" together with "overlap populations" [29]. This analysis was automatically produced by the used MNDO programs. Geometry optimizations were carried out using symmetry constraints, applied to bond stretchings and valence angles. Their definitions were based on symmetry of the planar molecular formula. To introduce appropriate molecular symmetry, different sets of repetitive units involving (or not) a central dummy atom were used [e.g., atom constraints containing an entire pyrrole (isoindole) cycle with *meso*-C(N) atoms, or proximate half-pyrrole (isoindole) atoms, separated by *meso*-C(N) atoms]. In all models, the *XY* plane was the plane of the molecule, and the inner hydrogen atoms in free-base molecules were aligned along the vertical *Y* axis. As a rule, the final optimized geometries from analogous MNDO computations were slightly different. Since the output orbital energy sets were totally shifted only by small values of 0.2–0.8 eV, the apparent dependence of the MNDO results from the introduced type of atomic constraints will be not discussed here.

The intermolecular energy of interaction between the pairs of molecules were computed and minimized using the DOCK command of the SYBYL software [30]. This method calculates the field of interactions on a grid, using the steric and electronic

contributions from the Tripos force field [31]. The energy of interaction for each atom of one molecule (ligand) is approximated by those of its nearest lattice point of the field generated by the second molecule (site) [32, 33]. We used a grid step of 0.1 Å.

Results and Discussion

1. Electron Populations, Bond Orders, and Geometries

Figures 1–6 give electron populations, bond orders, and bond lengths for the optimized structures of porphines and phthalocyanines. The model structures in Figure 1 represent symmetric distributions of charges as well as symmetric geometries. The aromaticity of the internal delocalized heteroatomic macrocycle is most pronounced for the ZnP complex. The metal-free porphines shown in Figure 2 have reduced symmetry. The aromaticity of the heteroatomic macrocycle is seriously altered, as well. H_2P presents a sequence of single and double bonds, as can be seen from bond orders and bond lengths. This aromaticity is partly regenerated by the presence of halogen atoms. The external five-membered ring has two purely single (1.486 Å) bonds and one double bond (1.373 Å). The aromaticity of the internal ring of the metal-free porphine dication (Fig. 3) is slightly disymmetric and the symmetry is not reflected in the electron population. As was already observed for ZnP, it seems that the electronic structure becomes very symmetric in the presence of a central metal ion; this observation is exemplified by the $PcAl^{1+}$, i.e., the monocationic Al–phthalocyanine complex (Fig. 4). The central macrocycle is highly aromatic, as reflected by bond orders and bond lengths. Nevertheless, the five-membered ring retains two single bonds that separate the external six-membered aromatic rings from the internal macrocyclic aromatic structure. The structures of H_2Pc and $H_2Pc(4N)$ molecules (Fig. 5) show less symmetry. Again, the external six-membered aromatic rings are separated from the macrocyclic aromatic system by pure single bonds. As can be seen, the addition of the pyridino ring modifies the internal system. Similar conclusions can be made for the tetrasulfonated phthalocyanines, the $H_2Pc(SO_3)_4^{4-}$ anion and the neutral $H_2Pc(SO_3H)_4$ shown on Figure 6. The metal-free ligands rarely exhibit symmetric electron populations and valency distribution, and often large deviations are observed (Figs. 5 and 6). Further comparison of the structures demonstrated in Figures 5 and 6 shows that sulfonation of the benzene ring does not alter the electron population of the inner cycle, but affects only positions adjacent to the S atom carbons. It is also seen that the net-negative charge in $H_2Pc(SO_3)_4^{4-}$ is localized on the O atoms of the sulfo groups and on the adjacent carbon atoms, but does not affect the electronic charge population of the entire macrocycle.

Although the optimized geometries of the porphine and phthalocyanine models do not match exactly the interatomic coordinates obtained by X-ray studies, the model structures resemble some important relations found in the experiment, e.g., the relatively long (single) bonds between C_α and C_β carbons of the pyrroles and the short (double) bonds between C_β and C_β atoms. Thus, the β-pyrrole carbons apparently are not coupled to the interior resonance system, in agreement with previous findings [34]. The same correlation is valid for the phthalocyanine macrocycle, where benzene rings are separated from the inner resonant system, in accordance with previously

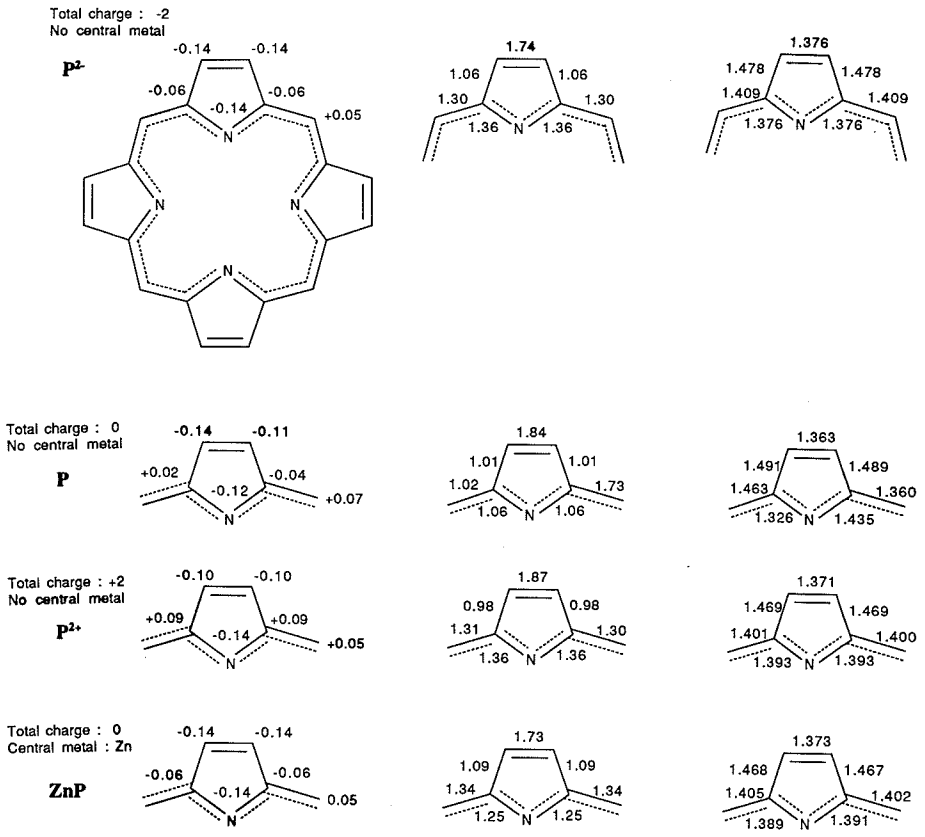

Figure 1. Electron population, bond orders, and bond lengths (Å) of symmetric (D_{4h}) porphine models: porphine dianion, P^{2-}; neutral porphine, P; porphine dication, P^{2+}; and Zn–porphine, ZnP.

published results [35]. An often discussed controversy concerns the positions of the central protons of the free-base porphine (phthalocyanine) structure (see, e.g., [6, 35, 36]). In the present models, these protons were kept arranged diametrically across the center of the molecules. Several structures were computed allowing proton nonplanar configuration in respect to the macrocycle plane (not shown). As a rule, the unrestricted models showed an overall tendency of out–off-plane bending, which was more pronounced in the case of the phthalocyanines and particularly in the presence of axial ligands. Since such structures often feature a lower heat of formation and HOMO energies, we assume that the planar arrangement represents one, but not necessarily the most stable, resonant structure of these molecules.

The *meso*-halogenated porphine derivatives have unique physico- and biochemical properties, which could reflect the apparent reduction of the induced inner ring current [37–39]. As can be seen from Figure 2, the presence of halogen atoms at *meso* positions of the macrocycle alters mainly the electron population between the halogen

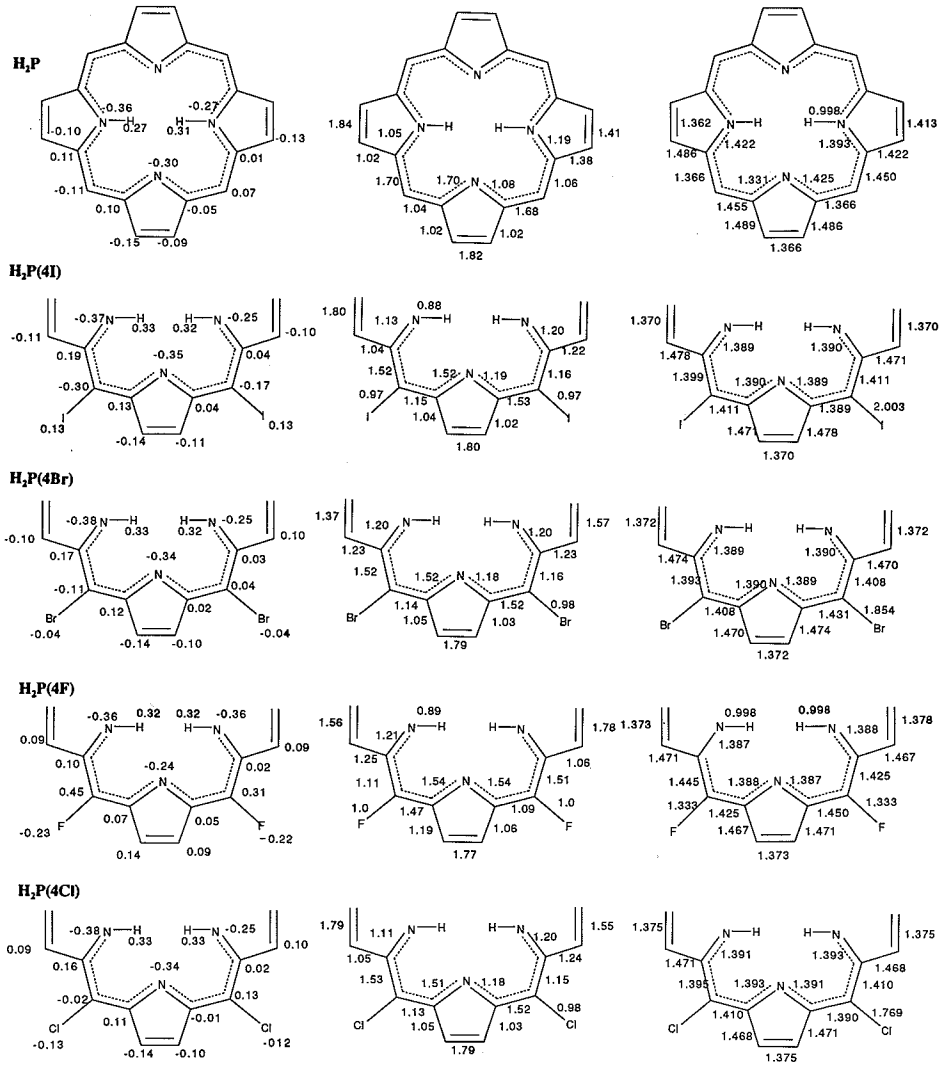

Figure 2. Electron population, bond orders, and bond lengths (Å) of metal-free porphine (H_2P) and *meso*-tetrahalogenated derivatives: $H_2P(4I)$, $H_2P(4Br)$, $H_2P(4Cl)$, and $H_2P(4F)$.

and *meso*-carbons. Furthermore, there are relationships between the nature of the halogen atom (electronegativity and van der Waals radius) and the change of the atomic charges on the α, β, γ, and δ carbons. These correlations are clearly visualized by the isopotential maps shown in Figure 7. The overall shapes of the isopotential contour of H_2P and $H_2P(4I)$ are rather symmetric and similar, while $H_2P(4F)$ and $H_2P(4Cl)$ display a distinct different positive/negative charge distribution, which is most likely due to the less expanded negative potential surface of the inner electron ring and the less symmetric tetrahalogen charges. The asymmetry of the charge distribution of

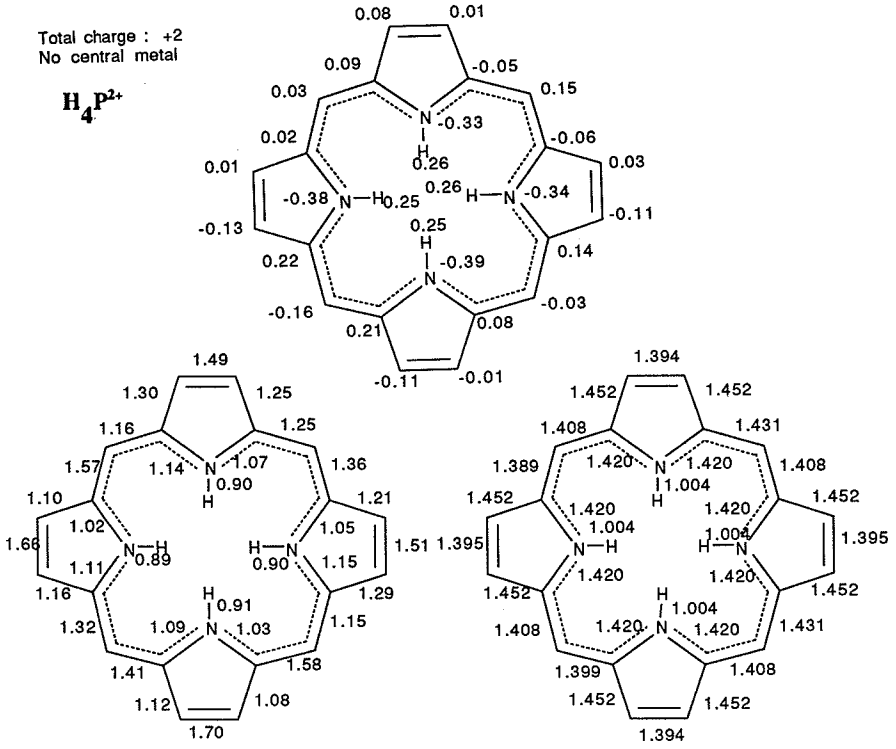

Figure 3. Electron population, bond orders, and bond lengths (Å) of metal-free porphine dication, H_4P^{2+} .

the $H_2P(4F)$ is evident from the form of the neutral contour shape. The asymmetry may infer the presence of several resonant structures of these compounds [37, 38]. The features of the $H_2P(4Br)$ isopotential map reflect a symmetry intermediate of the above two extremes (not shown).

2. *Molecular Orbital Structure and Energy Levels*

Tables I–III summarize the results from MNDO computations of the ground-state orbital energies (highest occupied and lowest virtual) of our molecular models, as well as present theoretical data obtained by other computational techniques. Analysis of the MO structure suggests the following: For all porphine derivatives, the HOMO and the closely related HOMO-1 (π A_u and π B_{1u}, in the case of H_2P and *meso*-halogenated derivatives) are separated from HOMO-2 by an energy gap of about 2.5–3.0 eV. The energy difference between HOMO and LUMO is much higher and ranges from 6.6 eV for neutral symmetric porphine to 5.6 and 5.3 eV for H_2P and ZnP, respectively. These MO features are in a very good agreement with those obtained by other quantum mechanical computations [3, 5, 6] as well as with the experimental values of the first ionization potential of porphyrins [40]. In general, however, our results show the

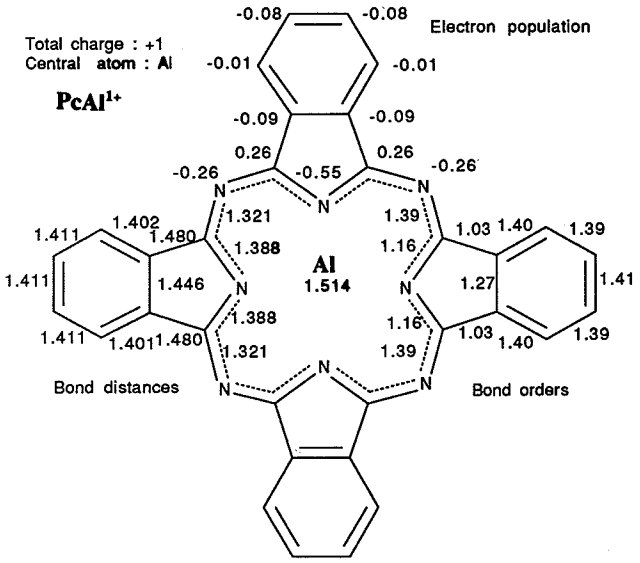

Figure 4. Electron population, bond orders, and bond lengths (Å) of Al–phthalocyanine monocation, $PcAl^{1+}$.

presence of a number of degenerated energy levels for orbitals lower than HOMO-3 and higher than LUMO+4. We suggest that this type of MO-clustering reflects the optimized geometry deviations from the true introduced molecular symmetry. A critical analysis of this band structure would require further calculations, including computations of the photo-cross sections of excited molecules to ascertain the line intensities. The energy levels of the HOMO and LUMO orbitals of H_2P are about 0.6 eV above those of the *meso*-halogenated H_2P derivatives, yet showing a similar energy gap. Interestingly, the relative energies of virtual orbitals LUMO+2, LUMO+3, and LUMO+4 of the halogenated derivatives are changed as compared to those of the parent molecule, in accordance with the expected (and experimentally observed) shifts in the Soret and Q band positions of these compounds [37].

The energy levels of phthalocyanine highest occupied and lowest empty orbitals are shown in Table III. In this case, HOMO (π A_u symmetry for H_2Pc) and HOMO-1 (π B_{1u}) are separated by 2.3–2.5 eV. The energy gap LUMO–HOMO is in the range of 4 eV. The positions of HOMO (6.59 eV) and HOMO-1 (8.93 eV) are in a good agreement with the recent VEH computations of the H_2Pc electronic structure and the experimental UPS/XPS spectra (Table III) [9, 10]. However, similarly to the case of porphine and its derivatives, the lower-lying orbitals (HOMO-2 and below) show band structuring. A comparable cluster-type MO structure has been reported previously for teraazaporphyrins (Hartree–Fock–Slater calculations) by Berkovitch-Yellin and Ellis [41]. When axial ligands were introduced in the computed models, no significant changes in the electron population and energy levels of the macrocycle were observed, although the electronic charge of the central metal atom was affected.

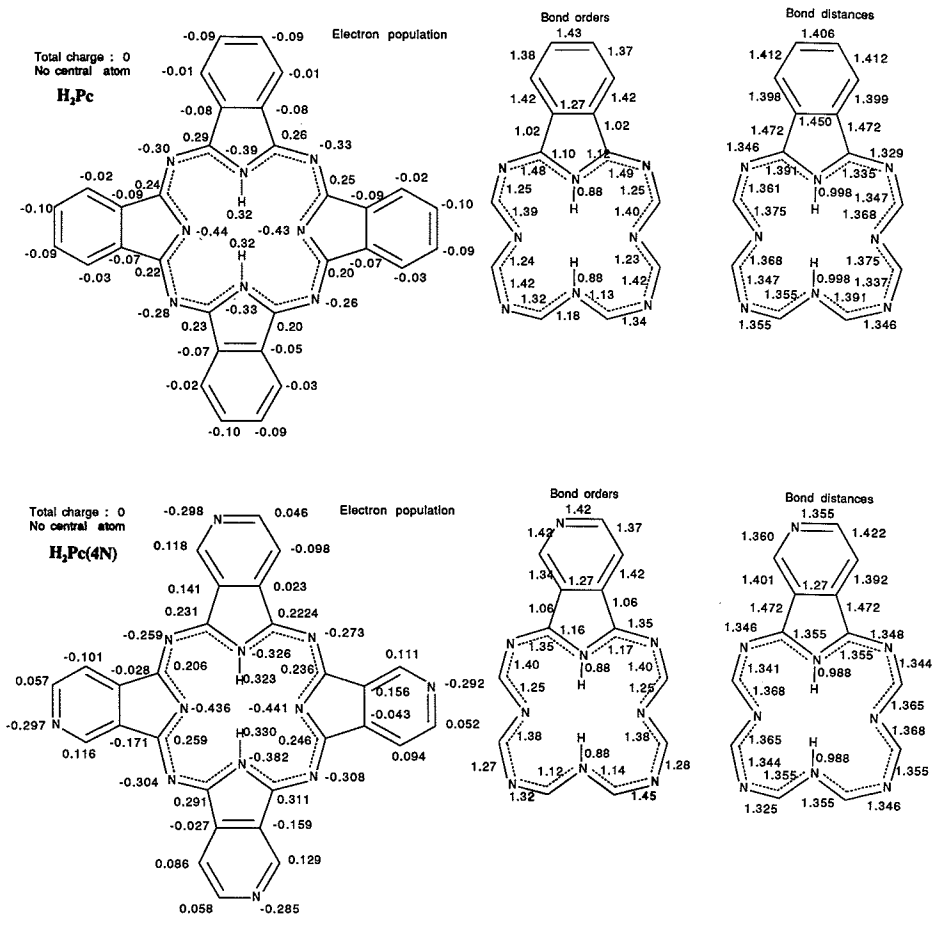

Figure 5. Electron population, bond orders, and bond lengths (Å) of free-base phthalocyanine, H_2Pc, and 2,3-tetra-2,3-pyridinoporphyrazine, $H_2Pc(4N)$.

3. Intermolecular Interactions of Porphine and Phthalocyanine Derivatives as Studied by Their Dimer Formation

Using the SYBYL force-field minimizing program, several different types of energy-favorable orientations of porphine and phthalocyanine dimers were obtained. The face-to-face offset geometry modes could be represented by two simple symmetry operations (Fig. 8): rotation of one of monomers around the Z axis (hereafter referred to as Type I geometry) and translation along the X (or Y) axis (referred to as Type II geometry), with an intermediate relative orientation of monomers assumed as combinations of these two modes, i.e., simultaneous slipping along X and/or Y axes and rotation about Z axis (Type III). The distance between the two monomers along the Z axis ranges between 2.8 and 3.4 Å (for neutral molecules). In general,

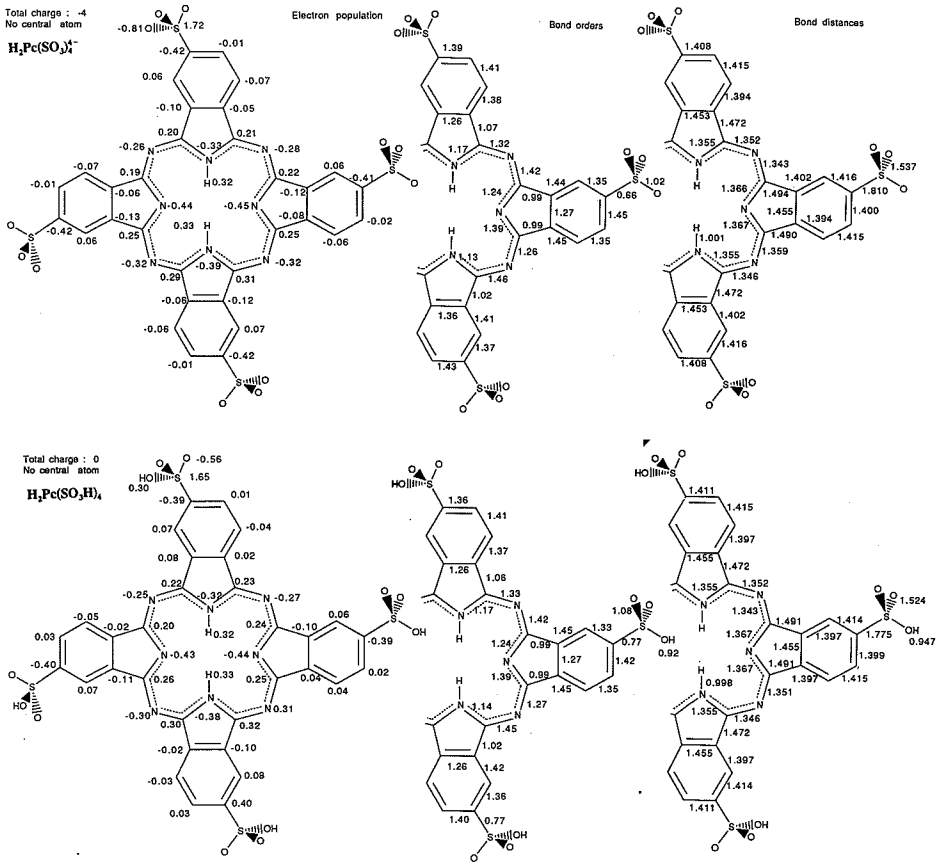

Figure 6. Electron population, bond orders, and bond lengths (Å) of free-base tetrasulfonated phthalocyanine tetracation, $H_2Pc(SO_3)_4^4$, and protonated neutral molecule, $H_2Pc(SO_3H)_4$.

for molecules that were experimentally known not to exist in dimeric (aggregated) form, the docking experiments resulted in noncofacial geometry with relative distances between monomers from 4 up to 25 Å, or more, with large repulsive electrostatic energy terms (see below). Table IV summarizes the data, including monomer energies (heat of formation), van der Waals attraction, and electrostatic repulsion/attraction terms. Some of the model molecules studied showed preference for more than one dimer orientation with close energy minima (ca. 1–2 kcal/mol). As can be seen from Figure 8 and Table IV, the plane-to-plane distance between uncharged monomers is determined by the sum of the van der Waals atom radii (~3 Å) and increases upon Br and I substitution. Only for Zn–porphine, the relative distance decreases to 2.8 Å, obviously reflecting the involvement of additional interatomic (electrostatic) interactions. The completely symmetrical uncharged molecule P showed the most symmetrical dimer orientation, represented by Type I orientation (45° rotation along Z axis) (Fig. 8). Other molecules for which the rotation along the Z axis (Type I)

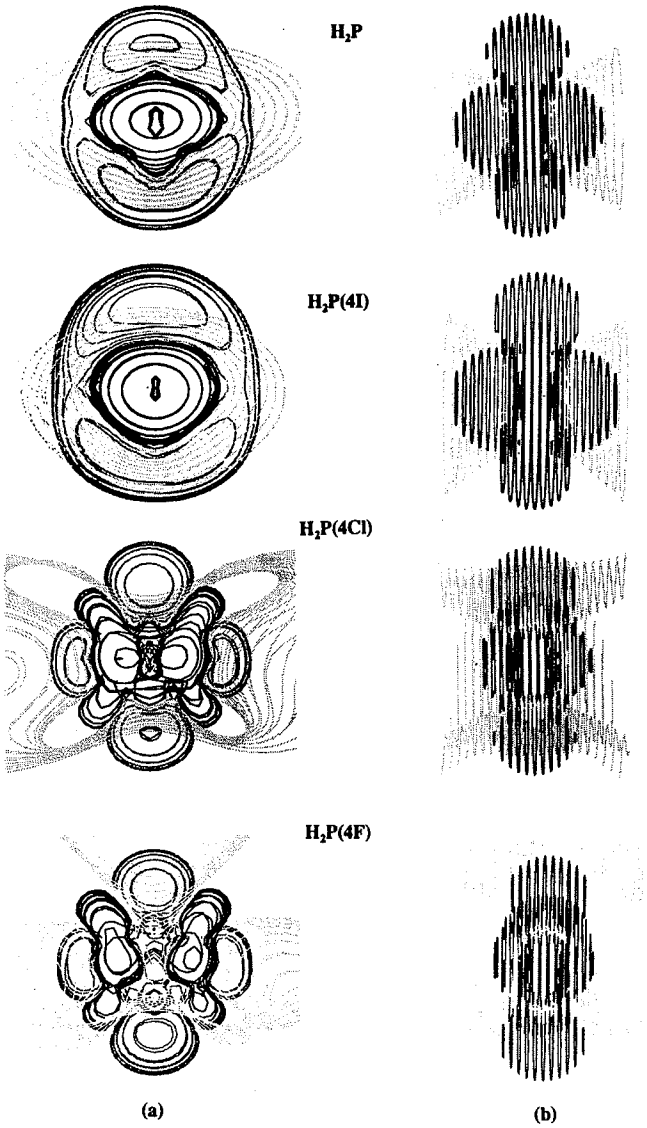

Figure 7. Isopotential maps of free-base, H_2P, and *meso*-tetrahalogenated porphine molecules: $H_2P(4I)$, $H_2P(4Cl)$, and $H_2P(4F)$. Line contours: high density (−1 kcal/mol), medium density (+1 kcal/mol), and low density (0 kcal/mol). Column (a), view along Oz axis; column (b), view along O*x* axis.

was obtained as preferential or one of possible orientations (but to a degree generally less than 45°) were $H_2P(4Cl)$, $H_2P(4F)$, $H_2P(4I)$, H_2Pc, and the "antiparallel" dimer of $H_2Pc(4N)$. Translation of one of the monomers along the *X* (or *Y*) axis was the most favorable orientation of the ZnP dimer. The slipping distance was about 2.9 Å and resulted in positioning of the Zn atom almost above the center of a pyrrole unit of

TABLE I. Electronic energies (in eV) of some of the highest-occupied and lowest-unoccupied molecular orbitals of various porphine derivatives: neutral porphine (P), porphine dianion (P^{2-}), and dication (P^{2+}); Zn–porphine (ZnP); and free-base porphine (H_2P).

Source	This work (MNDO)					PPP[a]	Ab initio[b]	CNDO[c]	
	Molecule and symmetry								
	P (D_{4h})	P^{2-} (D_{4h})	P^{2+} (D_{4h})	ZnP (D_{4h})	H_2P (D_{2h})	H_2P (D_{2h})	H_2P (D_{2h})	H_2P (D_{2h})	P^{2-} (D_{4h})
	2.117	9.121	−5.285	1.500	2.146	4.88	7.67		
	1.783	8.897	−5.307	1.407	1.436	3.68	5.72		
	1.536	8.340	−5.582	1.406	1.323	3.59	5.41		
	1.536	8.275	−6.730	1.344	1.245	3.19	5.05		
	1.467	8.054	−7.860	1.076	0.930	2.80	3.91		
	0.000	6.289	−7.862	−0.195	−0.294	0.81	1.36		
	−0.783	5.365	−10.242	−1.842	−1.681	−0.92	−1.41		
LUMO	−1.743	5.289	−10.514	−1.844	−1.818	−1.15	−1.84		
HOMO	−8.331	0.728	−15.857	−7.110	−7.389	−6.59	−8.00	−8.34	0.38
	−9.312	−0.523	−15.862	−7.422	−7.404	−6.67	−8.39	−8.59	−2.29
	−9.313	−2.046	−16.402	−9.657	−9.340	−8.49	−10.41	−11.79	−3.84
	−9.578	−2.066	−16.458	−9.658	−9.475	−8.74	−11.08	−12.04	−4.03
	−9.798	−2.433	−16.547	−9.723	−9.818	−9.62	−11.24	−12.17	−4.24
	−10.051	−2.798	−16.583	−9.931	−10.079	−9.94	−11.82	−12.43	−4.37
	−10.558	−2.964	−17.920	−9.933	−10.093	−9.94	−12.16	−13.25	−5.37
	−10.725	−3.118	−17.983	−10.008	−10.384	−9.98	−12.35	−13.40	−5.47
	−10.725	−3.121	−18.135	−11.164	−10.760	−11.21	−12.44	−14.41	−5.55
	−10.944	−3.190	−18.136	−11.225	−10.772	−12.27	−12.62	−14.50	−6.63
	−11.051	−3.347	−18.355	−12.494	−11.234	−12.80		−14.71	−7.08

[a][3].
[b][6].
[c][5].

TABLE II. Electronic energies (in eV) of some of the highest-occupied and lowest-unoccupied molecular orbitals of *meso*-halogenated porphine derivatives (symmetry D_{2h}).

	Molecule			
	$H_2P(4F)$	$H_2P(4Cl)$	$H_2P(4Br)$	$H_2P(4I)$
	1.502	0.769	0.749	0.708
	1.501	0.624	0.450	0.344
	0.941	0.480	0.362	0.323
	0.831	0.464	0.219	0.172
	0.603	0.219	0.204	0.155
	0.145	0.205	0.005	0.029
	−0.936	−0.982	−0.883	−0.995
	−2.312	−2.422	−2.337	−2.405
LUMO	−2.487	−2.480	−2.361	−2.464
HOMO	−7.799	−8.024	−7.849	−7.790
	−8.218	−8.100	−8.031	−8.168
	−9.856	−9.858	−9.762	−9.811
	−9.926	−9.943	−9.865	−9.942
	−10.131	−10.234	−10.107	−10.082
	−10.459	−10.511	−10.377	−10.331
	−10.663	−10.527	−10.395	−10.363
	−10.792	−10.921	−10.865	−10.756
	−11.327	−11.343	−11.075	−10.984
	−11.508	−11.537	−11.300	−11.176
	−11.524	−11.554	−11.311	−11.191
	−13.331	−12.625	−11.920	−11.197

the second molecule. Slipping along the $X(Y)$ axis (Type II) was observed for neutral and less symmetrical molecules, such as H_2P, $H_2P(4Cl)$, and $H_2P(4Br)$, with an offset translation distance smaller than that observed for the Zn−porphine. However, this geometry often was not unique, since other relative orientations of the monomers with similar energy minima were also observed (Table IV).

Comparison between the simplest symmetric structures, i.e., P and ZnP, shows that the van der Waals energy terms play a predominate role in the dimer formation, but the final geometry is controlled by the electrostatic interactions. Other molecules for which small attractive electrostatic terms contributed to a given dimer geometry were H_2P and $H_2P(4F)$. In most cases where no significant electrostatic attraction existed, more than one monomer orientation was found. The vector force-field diagrams obtained for the ZnP dimer show high Zn—N attractive interactions on both rings and, at closer distances, an electrostatic repulsion from peripheral protons. A three-dimensional diagram of the total molecular charge distribution (proportional to $\sum\sum|\Psi|^2$) of ZnP computed with the GRAPH output option of the MOPAC/SYBYL software showed that the orientation of the dimer was consistent with an alignment whereby the positively charged Zn atom (0.99 units) was positioned above the pyrrole π-cavity of the other molecule. It was furthermore obvious that the main contribution toward this interaction comes from the upper lying filled π-orbitals. Comparison of $\sum|\Psi|^2$ space

TABLE III. MNDO calculated energies (in eV) of some of the highest-occupied and lowest-unoccupied molecular orbitals of phthalocyanine derivatives.

	This work (MNDO)					VEH and experimental[a,b]	
	Molecule						
	H_2Pc (D_{2h})	$AlPc^{+1}$ (D_{4h})	$H_2Pc(SO_3H)_4$ (C_{2h})	$H_2Pc(SO_3)_4^{4-}$ (C_{2h})	H_2Pc4N (C_{2h})	H_2Pc (D_{4h})	Gas-phase potentials
	1.905	−1.882	−0.867	7.434	1.531		
	1.385	−2.122	−1.034	7.431	1.054		
	1.045	−2.133	−1.302	7.160	0.573		
	0.504	−2.300	−1.388	6.912	0.095		
	0.487	−2.384	−1.418	6.889	0.032		
	0.250	−2.611	−1.624	6.691	−0.129		
	0.157	−2.622	−1.893	6.602	−0.324		
	0.050	−3.250	−1.913	6.487	−0.392		
	−0.072	−3.260	−1.950	6.368	−0.567	ca. −3.0	
	−0.386	−3.343	−2.127	6.071	−0.790	ca. −3.2	
	−0.692	−4.043	−2.225	5.700	−1.157	ca. −3.8	
	−2.144	−5.317	−3.406	4.167	−2.701	ca. −4.9	
LUMO	−2.305	−5.325	−3.483	4.096	−2.789	ca. −5.1	
HOMO	−6.590	−9.468	−7.802	−0.247	−7.091	−6.41 (−6.32)	6.41
	−8.931	−11.937	−10.117	−2.607	−9.477	−8.77	8.75
	−9.331	−12.073	−10.601	−2.855	−9.862	−9.83	—
	−9.404	−12.088	−10.715	−2.880	−9.999	—	10.24
	−9.483	−12.120	−10.790	−2.887	−10.091	−11.06	11.20
	−9.514	−12.204	−10.892	−2.923	−10.359	−11.74	—
	−9.622	−12.246	−11.017	−2.927	−10.501	—	12.27
	−9.713	−12.275	−11.130	−2.982	−10.691	−12.99	12.57
	−10.053	−12.612	−11.282	−3.007	−10.926		
	−10.079	−13.350	−11.517	−3.022	−11.111		
	−10.874	−14.264	−11.534	−3.028	−11.142		

[a] [9].
[b] [10].

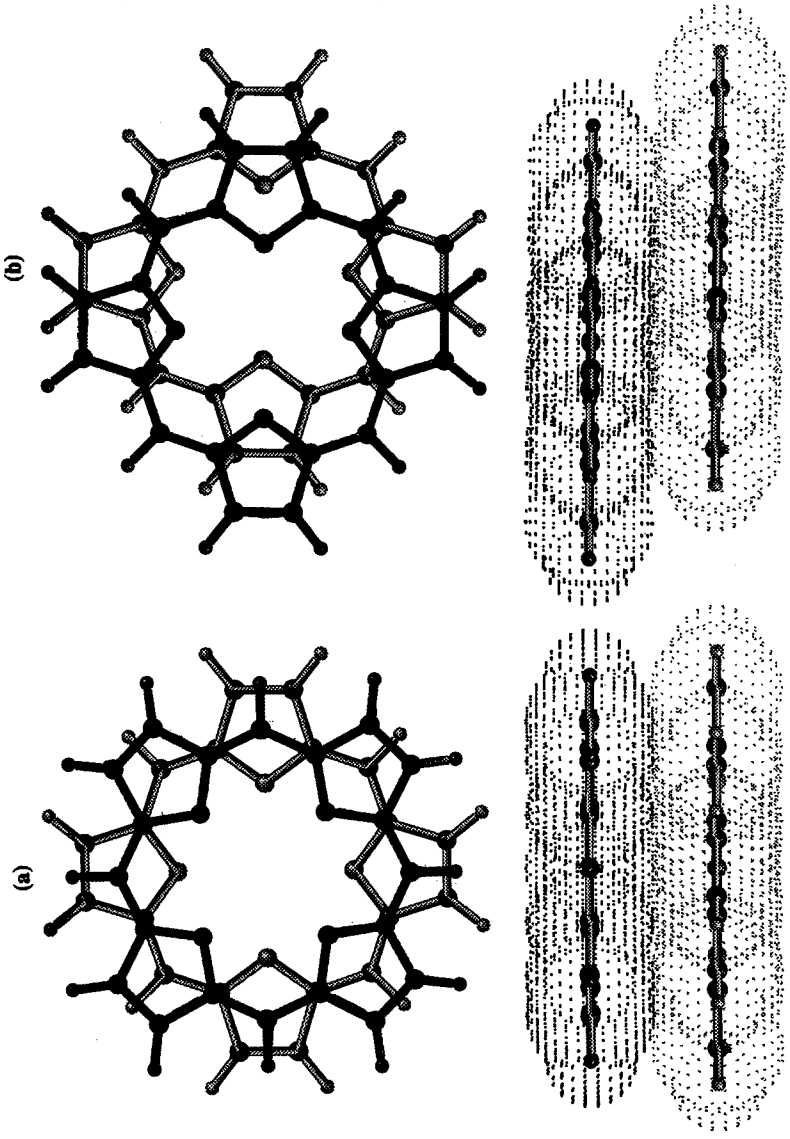

Figure 8. Relative orientations of monomers in two main porphine dimer structures: (a) rotation about Oz axis (Type I) and (b): translation along the Ox axis (Type II). Dotted clouds represent van der Waals radii.

TABLE IV. Heat of formation (ΔH) of the monomeric molecules (from MNDO [10]) in kcal mol^{-1} and the intermolecular interaction energy (decrease of the energy of the ligand when introduced in the field of the site) after intermolecular geometry minimization: electrostatic (El), van der Waals (VDW), and their difference (ΔE), plane-to-plane distances d(Å), and type of the relative monomer-to-monomer orientation.

Molecule	Symmetry	Charge	ΔH	VDW	El	ΔE	d(Å)	Orientation
P	D_{4h}	0	243.0	−22.5	+2.4	−20.1	3.02	I (45° about Oz)
ZnP	D_{4h}	0	193.8	−20.6	−5.0	−25.6	2.83	II (2.8 Å along Ox or Oy)
H_2P	D_{2h}	0	206.2	−20.2	−1.2	−21.4	3.00	II (1.2 Å along Ox)
$H_2P(4I)$	D_{2h}	0	279.7	−32.8	+7.8	−25.0	3.35	I (30° about Oz)
$H_2P(4Br)$	D_{2h}	0	234.7	−29.6	+1.2	−28.4	3.10	II (1.8 Å along Ox)
				−20.6	+0.7	−19.9	3.12	III
$H_2P(4Cl)$	D_{2h}	0	192.8	−29.2	+0.1	−29.1	3.01	II (1.5 Å along Oy)
				−28.2	+1.4	−26.8	3.00	I (45° about Oz)
$H_2P(4F)$	D_{2h}	0	36.3	−24.9	−1.2	−26.1	3.00	I (135° about Oz) and III
P^{2+}	D_{4h}	+2	679.4	−13.4	+28.1	+14.7	3.20	No preference[a]
H_4P^{2+}	D_{2h}	+2	560.7	−13.6	+26.0	+12.4	4.80	No preference[a]
H_2Pc	D_{2h}	0	270.0	−38.4	+3.4	−35.0	3.00	I (17° about Oz)
$H_2Pc(4N)$[b]	C_{2h}	0	308.1	−35.7	+1.9	−33.8	3.00	III
$H_2Pc(4N)$[c]				−36.5	+2.4	−34.1	3.00	I (17° about Oz)
$AlPc^{+1}$	D_{4h}	+1	329.5	−34.7	+3.4	31.3	2.90	III

[a]Weak attraction.
[b]Symmetric orientation of molecules in respect to pyridine N atoms.
[c]Antisymmetric orientation of molecules in respect to pyridine N atoms.

diagrams of HOMO and HOMO-1 orbitals of P and ZnP (Fig. 9) suggests that the van der Waals energy term most likely arises from electrons on both HOMO and HOMO-1; in contrast, the Zn electrostatic contribution and the sequential dimer geometry results from the HOMO-1 electrons only.

Our results for ZnP are in good agreement with experimental data and theoretical considerations on the dimer structure of side-chain unsubstituted metalloporphyrins [18, 42]. The apparent differences between the ZnP dimer energy obtained in the above-referred studies and our estimated interaction energies ($\approx$10 kcal/mol) most likely reflect different charge distribution assignments and/or the influence of solvatation. We used MOPAC/MNDO Mulliken-type charge population analysis and a definition of the van der Waals interaction energy based on Lennard–Jones potential. On the other hand, our models predict a dimer geometry of π-stacked nonmetalated prophines of another type (rotation about the Oz axis [Type I] or mixed rotation/translation [Type III], Table IV). In the previous theoretical study [18], such dimer orientation was rejected as energy unfavorable, but the authors apparently did not considered the effects of peripheral or inside hydrogen atoms. From the isopotential maps, it was possible to visualize the contribution of the peripheral substituents (including halogen atoms in the *meso*-position) in the spanning of the positive isopotential contour (see, e.g., Fig. 7). For nonhalogenated derivatives, the orientation-dependent proton repulsion was also obvious from the vector force-field diagrams (not shown). In parallel, increased attractive van der Waals interactions in the presence of large halogen atoms (I, Br, Cl) are also obvious (Table IV), which, as a rule, altered the type of the dimer geometry. It should be noted that intermolecular interactions resulting in Type I geometry have been reported for crystal structures of benzoquinones with symmetry similar to that of some of our models (e.g., H_2P, H_2Pc, etc.) [43]. The predicted preferential Type I geometry of Pc dimers is also in line with previous experimental data obtained for some Pc derivatives [44], although the rotation angle about the Z axis in our models is smaller.

For all phthalocyanine models, an increase of van der Waals terms in the interaction energy is consistent with the more expanded π-electron character. $AlPc^{1+}$ was the only charged molecule that still showed dimer formation with a well-defined geometry. This is an interesting result, since the positive charge on the Al atom is relatively high (1.5 units, Fig. 4), but the electrostatic repulsion obviously is not enough to overcome the large van der Waals attraction. The docking of negatively charged porphine and phthalocyanine derivatives resulted in high repulsion of the ligand molecule (often more than 15 Å). The isopotential map contours of these molecules (e.g., -1 kcal/mol isopotential surfaces), which were almost spherical in shape, spanned over 10 Å. At these distances, of course, the van der Waals terms vanish. A tendency of dimer formation was also found for the positively charged symmetric molecules, P^{2+} and H_4P^{2+}, but because of the weak attraction and pronounced repulsion, these were not unique orientations (Table IV). Tetrasulfophthalocyanines, as well as all metalloderivatives, bearing in addition two axial ligands (Cl, OH) did not show the presence of predominant attractive interactions and specified face-to-face dimer geometry.

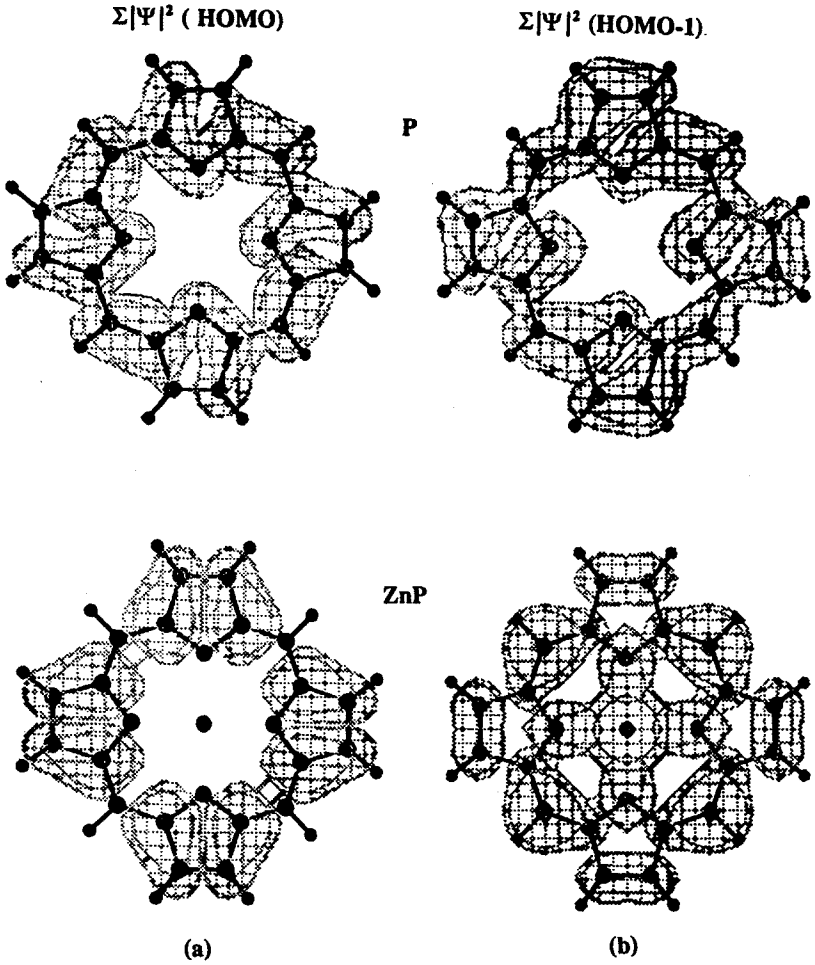

Figure 9. Neutral symmetric porphine, P, and Zn–porphine, ZnP, electronic charge density diagrams of the two highest-occupied molecular orbitals: $\sum|\Psi|^2$ (HOMO) (a); and $\sum|\Psi|^2$ (HOMO-1) (b).

Concluding Remarks

In this work we performed semiempirical (MNDO) molecular orbital calculations to characterize electronic and geometry properties of various porphine and phthalocyanine derivatives. Subsequently, these models were utilized to study intermolecular interactions (ground-state dimerization). The results show that the variations of electronic properties as a function of the introduced symmetry, molecular charges, and inner and/or peripheral substituents, determine in a predictable way the rate and extent of the intermolecular interactions, with the two energy components, van der Waals and electrostatic terms, evaluated separately. In most cases, we achieved reasonable agreement with previous theoretical and experimental data. These models can be

further refined to perform calculations of the excited-state orbital populations, which would allow direct comparison of the theoretical results with known spectroscopic properties of porphyrin and phthalocyanine dimers (aggregates) in solution. Obviously, further work is required to introduce solvent-dependent effects as well.

Acknowledgments

This work was supported by the Natural Sciences and Engineering Research Council of Canada (A. G. M.) and the Medical Research Council of Canada (J. E. V. L., T. G. G). The authors acknowledge the Computer Service of the University of Sherbrooke for their generous allocation of computer time. This research was made possible by the support of IBM Canada Limited Company (Cooperative Research Projects).

Bibliography

[1] M. Gouterman, in *The Porphyrins,* D. Dolphin, ed. (Academic Press, New York, 1977), Vol. III, Chap. 1.
[2] C. Weiss, H. Kobayashi, and M. Gouterman, J. Mol. Spectrosc. **16**, 415 (1965).
[3] M. Sundbom, Acta. Chem. Scand. **22**, 1317 (1968).
[4] M. Zerner and M. Gouterman, Theor. Chim. Acta **4**, 44 (1966).
[5] G.M. Maggiora, J. Am. Chem. Soc. **95**, 6555 (1973).
[6] J. Almlöf, Int. J. Quantum Chem. **8**, 915 (1974).
[7] J.D. Petke, G.M. Maggiora, L. Shipman, and R. Christoffersen, J. Mol. Spectros. **71**, 64 (1978).
[8] U. Nagashima, T. Takada, and K. Ohno, J. Chem. Phys. **85**, 4524 (1986).
[9] E. Orti and J.L. Brédas, J. Chem. Phys. **89**, 1009 (1988).
[10] E. Orti, J.L. Brédas and C. Clarisse, J. Chem. Phys. **92**, 1228 (1990).
[11] J.E. van Lier and J.D. Spikes, *Photosensitizing Compounds: Their Chemistry, Biology and Clinical Use,* Ciba Foundation Symposium 146, G. Bock and S. Harnett, Eds. (Wiley, New York, 1989), pp. 17–32.
[12] M.B. Shopova and T.G. Gantchev, J. Photochem. Photobiol. (B) **6**, 49 (1990).
[13] T.G. Gantchev, M.G. Kaltchev, and G.P. Gotchev, Int. J. Radiat. Biol. Relat. Stud. Phys. Chem. Med. **60**, 597 (1991).
[14] T.R. Janson and J.J. Katz, J. Magn. Res. **6**, 209 (1972).
[15] R.J. Abraham, F. Eivazi, H. Pearson, and K.M. Smith, J. Chem. Soc., Chem. Commun. 699 (1976).
[16] A.V. Muehldorf, D. van Engen, J.C. Warner, and A.D. Hamilton, J. Am. Chem. Soc. **110**, 6561 (1988).
[17] H.J. Schneider, K. Philippi, and J. Pöhlmann, J. Angew. Chem., Int. Ed. Engl. **23**, 908 (1984).
[18] C.A. Hunter and J.K.M. Sanders, J. Am. Chem. Soc. **112**, 5525 (1990).
[19] M.J.S. Dewar and W. Thiel, J. Am. Chem. Soc. **99**, 4899 (1977).
[20] M.J.S. Dewar and W. Thiel, J. Am. Chem. Soc. **99**, 4907 (1977).
[21] D.M. Collins and J.L. Hoard, J. Am. Chem. Soc. **92**, 3761 (1970).
[22] J.M. Robertson, J. Chem. Soc. 1195 (1936).
[23] R. Bonnett, I.A.D. Gale, and G.F. Stephenson, J. Chem. Soc. (C) 1600 (1966).
[24] H. Ali and J.E. van Lier, Tetrahedron Lett. **38**, 5015 (1991).
[25] *MOPAC. A General Molecular Orbital Package* (QCPE program no 455) (The Quantum Chemistry Program Exchange, Department of Chemistry, Indiana University, Bloomington, IN 47405, 1990).
[26] L.P. Davis, R.M. Guidry, J.R. Williams, M.J.S. Dewar, and H.S. Rzepa, J. Comp. Chem. **2**, 433 (1991).
[27] M.J.S. Dewar and H.S. Rzepa, J. Comp. Chem. **4**, 158 (1983).
[28] M.J.S. Dewar and K.M. Merz, Organometallics **5**, 1494 (1986).
[29] R.S. Mulliken, J. Chem. Phys. **23**, 1833 (1955).
[30] *SYBYL. Molecular Modelling Software,* Version 5.4, (1991), Tripos Associates, St. Louis, MO 63144 (1991).
[31] M. Clark, R.D. Cramer III, and N. Van Opdenbosch, J. Comp. Chem. **10**, 982 (1989).
[32] P. Goodford, J. Med. Chem. **28**, 849 (1985).

[33] P. Goodford, in *Computer-Aided Molecular Design,* W. G. Richards, Ed. (Oxford University Press, Oxford, U.K., 1989), Chap. 12, p. 147.
[34] L. E. Webb and E. B. Fleischer, J. Am. Chem. Soc. **87**, 667 (1965).
[35] B. F. Hoskins and S. A. Mason, Chem. Commun. 554 (1969).
[36] B. H. Meier, C. B. Storm, and W. L. Earl, J. Am. Chem. Soc. **108**, 6072 (1986).
[37] J.-H. Fuhrhop, *The Porphyrins,* D. Dolphin, Ed. (Academic Press, New York, 1978), Vol. II, Part B, Chap. 5.
[38] H. Toi, M. Homma, A. Suzuki, and H. Ogoshi, J. Chem. Soc., Chem. Commun. 1791 (1985).
[39] A. Ando, T. Shinada, S. Kinoshita, N. Arimura, M. Koyama, T. Nagai, T. Miki, I. Kumadaki, and H. Sato, Chem. Pharm. Bull. **38**, 2175 (1990).
[40] A. Stanienda, Z. Naturforsch. **B23**, 1285 (1968).
[41] Z. Berkovitch-Yellin and D. E. Ellis, J. Am. Chem. Soc. **103**, 6066 (1981).
[42] C. A. Hunter, M. N. Meah, and J. K. M. Sanders, J. Am. Chem. Soc. **112**, 5773 (1990).
[43] D. Rabinovich and G. M. J. Schmidt, J. Chem. Soc. (B) 144 (1967).
[44] N. S. Hush and A. S. Cheung, Chem. Phys. Lett. **47**, 1 (1977).

Received June 2, 1992
Revised manuscript received August 3, 1992
Accepted for publication October 20, 1992